Applied Mathematics and Mechanics
(English Edition, Vol. 16, No. 10, Oct. 1995)

Published by SU,
Shanghai, China

THE ANALYTICAL STUDY ON THE LASER INDUCED REVERSE-PLUGGING EFFECT BY USING THE CLASSICAL ELASTIC PLATE THEORY (I)—TEMPERATURE FIELDS*

Zhou Yichun (周益春)[1] Duan Zhuping (段祝平)[1] Wang Chunqui (王春全)[1]

(Received Aug. 31, 1994)

Abstract

The temperature distributions in the metallic foils induced by spatially cylindrical long-pulsed laser is examined in order to analyse the newly-discovered reverse-plugging effect (RPE). An exact solution for the temperature fields is derived by using the Hankel transform and Laplace transform. Numerical results are obtained for both spatial distributions with Gaussian and cylindrical types. The results show that the spatially cylindrical distribution of laser offers a formidable potential for the RPE.

Key words long pulsed laser, the RPE, temperature fields

I. Introduction

Because of its special properties, intense laser has attracted a great deal of attentions over the last few years, for those people working in the fields of material structure damage mechanism and laser processing. As well known, the interaction of laser with materials usually leads to two types of damage, mechanical and thermal damage, each depending mainly on the laser parameters such as laser intensity and pulse duration[1-6] When a continuous wave laser with relatively low intensity of the order of $10^4 w/cm^2$ or less irradiates on the surface of a solid target, a fraction of laser energy is absorbed by the target material, heating up it to generate a heat-affected zone. Also, such localized and nonuniform heating may cause a great amount of thermal stress. If the thermal stress exceeds the high temperature fracture strength of the material, it may lead to damage and fracture in the heated zone of material. If the laser intensity is on the order of $10^5 \sim 10^8 w \cdot cm^2$ and the pulse duration is on the order of milliseconds, the main phenomena are melting and vaporization. They may punch a hole and result in stress concentration and material structure fracture. In addition, the irradiation of the laser of very high intensity ($10^{10} w/cm^2$ or more) and of short pulse duration (several nanoseconds) may lead to the formation of plasma on the surface of solid materials. In turn, the plasma can interact with the laser beam and generate shock wave propagating into the target. Even before the laser pulse is over, ablation on the target surface drops and a sequence

*Project supported by the Field of Laser Technology of the National High-Tech. Research and Development Programme, i.e., the 863 plan.

[1] Laboratory for Nonlinear Mechanics of Continuous Media (LNM), Institute of Mechanics, Chinese Academy of Sciences, Beijing 100080, P. R. China

of rarefaction waves propagates into the target, overtaking and attenuating the shock wave. This shock wave will be reflected from the free surface of the target and cause spall above threshold amplitudes.

Besides the above-mentioned types of damage, we have observed experimentally a new type of damage, i.e., the RPE, in the studying of the interaction of a long pulse laser with metallic foils[7-8]. The RPE can be briefly described as follows. When the laser beam with the intensity in the range of $10^5 \sim 10^6 w/cm^2$ and pulse duration of 0.3ms irradiates on the surface of H65 copper alloy and aluminum alloy foils with 0.09mm and 0.055mm in thickness, they will bulge in the direction opposite to the laser incident direction. And later the foils exhibit the thermo-plastic shear deformation localization on the rim of laser irradiation region. Then a serious thermal micro-to-macro damage and a plugging-like failure will take place at a very narrow region (about 10μm in width) as the laser energy gradually increases. The failure model looks like general plugging effect (GPE), which happens in a thin plate penetrated normally by a long rigid projectile. In the GPE the plugging direction is identical to the projectile moving direction, while in the RPE the plugging direction is opposite to the laser incident direction. To the best of our knowledge, this phenomenon has not been reported in open literatures.

The understanding of the mechanism of the RPE is specially essential when the laser is considered as a tool of material processing. The studying of the RPE is also important for controlling laser parameters to produce material damage in an optimum way. The discovery of the RPE may provide engineers and scientists with a new method to study the nonadiabatic shear deformation localization. The present study explores the characteristics of temperature distribution and its dependence on laser intensity, temporal and spatial distribution of pulse laser beam. The next section outlines the laser parameters used in the experiment. Section III outlines analytically the solution of corresponding heat-diffusion equation. Appropriate calculations of the thermal profiles and some discussions are given in detail in Section IV. We conclude in Section V with a summary of the distinguished features of the present study.

II. Laser Parameters Employed in Test

Our experiments on the RPE was conducted by using a multi-mode, single-pulse Nd:Glass laser with the wavelength 1.06μm. The instrument was introduced in [9] in detail. The diagnostics include routine monitoring of beam characteristics, such as energy and temporal and spatial shapes.

The typical temporal shape shown in Fig. 1 was measured by PIN photoelectric cell with a corresponding response time less than 1.0ns. From the figure one can see that laser intensity rises rapidly within 50μs-rising time, and decays exponentially. The full width at half maximum (FWHM) of pulse laser is about 250μs. The temporal shape of laser pulse shows the characteristics of multi-pulse sequence. For the convenience of theoretical analysis, we fit the temporal shape with an analytical formula

$$g(t) = e^{-\alpha t}(1 - e^{-\beta t}) \tag{2.1}$$

where the constant α and β are, respectively, $1.5 \times 10^4 s^{-1}$ and $8.0 \times 10^4 s^{-1}$, and t time. And thus, laser power P and its energy E_J can be, respectively, expressed by

$$P' = P'_{max} g(t), \quad E_J = \frac{\beta}{\alpha(\alpha+\beta)} P'_{max} \tag{2.2}$$

where P_{max} is the maximum power.

Meanwhile, the spatial distribution of laser beam was probed by charge-coupled device (CCD) sensors with 512×512 elements. The CCD camera is a sensitive programmable instrument with electronic digitized readout connected to a microcomputer for exact and fast data acquisition and handling. In order to make the CCD sensors work linearly, the software module make it necessary that the ratio of maximum power intensity I_{max} to minimal power intensity I_{min} is less than 50.0. It is sure that the relative error of signal measured by the CCD camera is less than 2%. Solid-state CCD devices are capable of integration and storage of the data. Modern imaging CCD detector systems offer many exciting features of laser beam for our theoretical studying the RPE. The two and three dimensional shapes of the spatial distribution are, respectively, shown in Fig. 2 (a) and (b). The profile of laser spatial distribution is of non-Gassian type and roughly uniform within the laser spot and declines very rapidly at the edge of laser beam. In other words, the spatial distribution of laser is of cylindrical type. The cylindrical function is used to describe the spatial shape of the laser beam

$$f(r)=\begin{cases}1, & 0\leqslant r\leqslant a\\ 0, & r>a\end{cases} \tag{2.3}$$

where r is radial coordinate and a is radius of laser spot. The spatial shape of Gaussian type of single-mode laser is

$$f(r)=\exp[-(r/a)^2], \qquad 0<r<\infty \tag{2.4}$$

where a also is radius of laser spot.

III. Temperature Fields

A. Governing equations

In the present study, we model the temperature distributions of a conducting film subjected to a laser pulse with a given temporal and spatial distributions. Four assumptions in the present study are made below:

(1) The laser beam is taken as surface heat supply to the film. Besides, there is no other heat supply to the film. The assumption is reasonable because the laser energy only deposits on the surface and the depositing depth is on the order of several micrometers for metals such as aluminum and copper.

(2) The non-irradiated surface of film is thermally isolated. Meanwhile, the place where the radial cooradiate is b retains ambient temperature T_∞. This assumption matches closely real situation in short time when the heat conduction distance in the radial direction is much shorter than the laser spot radius.

(3) All material parameters are constant. Strictly speaking, all material parameters, such as thermal diffusivity D, thermal conductivity k and reflectivity R_∞ are temperature-dependent, consequently, time-dependent. Fortunately, the material parameters vary slowly with temperature T if there is no phase transformation. When the laser intensity is not too high, saying between $10^5\sim10^6$w/cm^2, there is no solid-to-liquid phase transformation during the laser irradiation. The determination of reflectivity R_∞ is very difficult. The actural dependence of R_∞ on material parameters and laser parameters would be deterimined both experimentally and theoretically.

(4) The problem is studied in a static coordinate system and the temperature and deformation of thin plate are uncoupled.

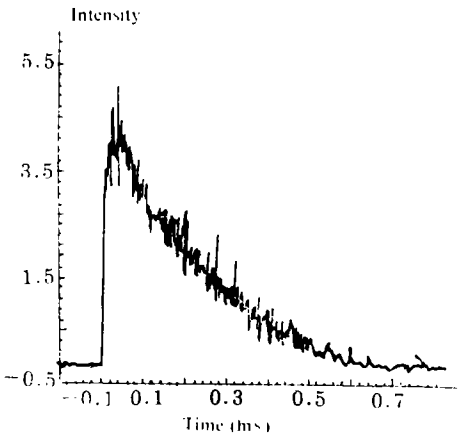

Fig. 1 The temporal shape

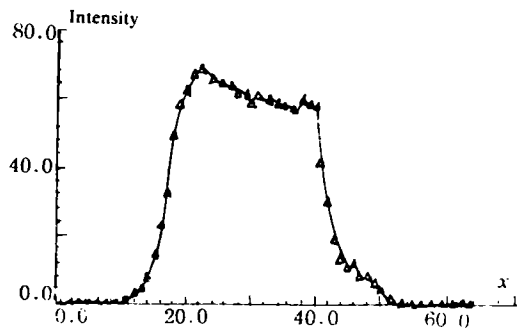

Fig. 2(a) The two dimensional shapes

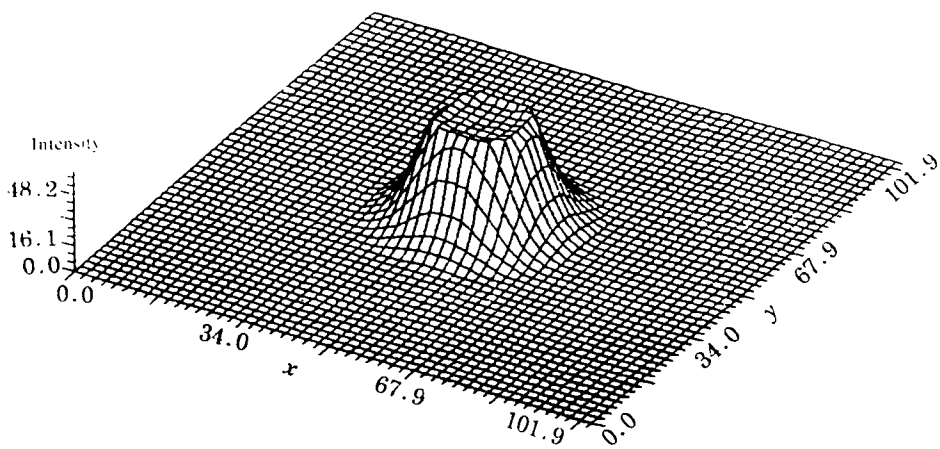

Fig. 2(b) The three dimensional shapes

Fig. 3 shows the geometric configuration of structure studied here. The cylindrical coordinate system (r, z) is at the middle plane, where r and z are coordinate, respectively, in the radial and the axial directions. The front surface of the thin plate is irradiated by a laser beam. Under above-mentioned assumptions, the governing equations in (r, z) system are, respectively, expressed in the following:

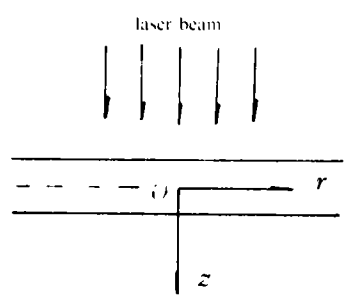

Fig. 3 The coordinate system

heat-diffusion equation

$$\frac{\partial^2\theta}{\partial r^2}+\frac{1}{r}\frac{\partial\theta}{\partial r}+\frac{\partial^2\theta}{\partial z^2}=\frac{1}{D}\frac{\partial\theta}{\partial t} \tag{3.1}$$

initial condition

$$\theta|_{t=0}=0 \tag{3.2}$$

boundary condition

$$-k\frac{\partial\theta}{\partial z}\Big|_{z=-h/2}=\frac{(1-R_0)}{\pi a^2}P_{\max}f(r)g(t)\quad -k\frac{\partial\theta}{\partial z}\Big|_{z=h/2}=0 \tag{3.3}$$

$$\partial\theta/\partial r|_{r=0}=\theta|_{r=b}=0 \tag{3.4}$$

where $\theta=T-T_0$, T, b are, respectively, temperature rise, temperature, the radius of specimen. To solve the genernal heat diffusion equation, the quasi-linearization of Eq. (3.1) is made by employing Kirchhoff's transform

$$\Theta=k_0^{-1}\int_{T_0}^{T}k(\xi)d\xi \tag{3.5}$$

where k_0 is the thermal conductivity measured at the ambient temperature T_0. The variable Θ is known as the linear temperature. Inserting Eq. (3.5) into Eq. (3.1) leads to a quasi-linearized heat-diffusion equation

$$\frac{\partial^2\Theta}{\partial r^2}+\frac{1}{r}\frac{\partial\Theta}{\partial r}+\frac{\partial^2\Theta}{\partial z^2}=\frac{1}{D}\frac{\partial\Theta}{\partial t} \tag{3.6}$$

Consequently, the initial and boundary conditions (3.2)—(3.4) are rewritten as follows:
initial condition

$$\Theta|_{t=0}=0 \tag{3.7}$$

boundary condition

$$-k_0\frac{\partial\Theta}{\partial z}\Big|_{z=-h/2}=\frac{(1-R_0)}{\pi a^2}P_{\max}f(r)g(t)-k_0\frac{o\Theta}{\partial z}\Big|_{z=h/2}=0 \tag{3.8}$$

$$\partial\Theta/\partial r|_{r=0}=\Theta|_{r=b}=0 \tag{3.9}$$

Strictly speaking, Eq. (3.6) is not linear since D is temperature dependent as well. In fact, D varys slowly with temperature and is appromately temperature-independent. This makes Eq. (3.6) be quasi-linear. Hence, the elimination of the temperature-dependence of k reduces considerably the complexity of the problem.

For convenience in the subsequent analysis, the dimensionless variables are introduced as follows

$$\hat{\Theta}=\frac{\Theta}{h_4T_m},\quad \hat{t}=\frac{tD}{a^2}=\frac{t}{t_0},\quad \hat{r}=\frac{r}{a},\quad \hat{z}=\frac{z}{a} \tag{3.10}$$

where T_m is the melting temperature of material and $t_0=a^2/D$. Meanwhile, other dimensionless parameters are defined in the following

$$\left.\begin{aligned} &A=\frac{\alpha a^2}{D},\quad B=\frac{(\alpha+\beta)a^2}{D},\quad h_1=\frac{h}{a}\\ &h_2=\frac{b}{a},\quad h_4=\frac{(1-R_0)P_{\max}}{k_0\pi aT_m}\end{aligned}\right\} \tag{3.11}$$

For the convenience of writting in the subsequent derivation, the dimensionless variables $\hat{\Theta}$, $\hat{r}$, $\hat{z}$ and $\hat{t}$ are, respectively, replaced by Θ, r, z and t. The governing equations of temperature fields are expressed in dimensionless form as follows:
heat-diffusion equation

$$\frac{\partial^2\Theta}{\partial r^2}+\frac{1}{r}\frac{\partial\Theta}{\partial r}+\frac{\partial^2\Theta}{\partial z^2}=\frac{\partial\Theta}{\partial t} \tag{3.12}$$

initial condition

$$\Theta|_{t=0}=0 \tag{3.13}$$

boundary condition

$$\left.\frac{\partial\Theta}{\partial z}\right|_{z=-h_1/2}=-f(r)g(t),\quad \left.\frac{\partial\Theta}{\partial z}\right|_{z=h_1/2}=0 \tag{3.14}$$

$$\partial\Theta/\partial r|_{r=0}=\Theta|_{r=h_2}=0 \tag{3.15}$$

Consequently, the temporal shape (2.1) and the spatial shape (2.2) and (2.3) are rewritten in the dimensionless form as follows:
temporal shape

$$g(t)=e^{-At}-e^{-Bt} \tag{3.16}$$

spatially cylindrical shape

$$f(r)=\begin{cases}1, & 0\leqslant r\leqslant 1\\ 0, & r>1\end{cases} \tag{3.17}$$

spatially Gaussian shape

$$f(r)=\exp[-r^2],\qquad 0<r<\infty \tag{3.18}$$

B. The solution of the temperature fields

Referring to the boundary condition (3.15), let Θ be expanded in terms of zeroth order Bessel function

$$\Theta=\sum_{k_n}\Theta^*(k_n,z,t)J_0(k_nr) \tag{3.19}$$

where k_n is the roots of equation $J_0(k_nh_2)=0$. Inserting the expanded expression (3.19) into (3.12)−(3.14), we obtain the differential equation on the unknown variable $\Theta^*(k_n, z, t)$ together with the initial and boundary conditions

$$-k_n^2\Theta^*+\frac{\partial^2\Theta^*}{\partial z^2}=\frac{\partial\Theta^*}{\partial t} \tag{3.20}$$

$$\Theta^*|_{t=0}=0 \tag{3.21}$$

$$-\left.\frac{\partial\Theta^*}{\partial z}\right|_{z=-h_1/2}=\frac{2f^*(k_n)g(t)}{h_2^2J_1^2(k_n,h_2)},\quad \left.\frac{\partial\Theta^*}{\partial z}\right|_{z=h_1/2}=0 \tag{3.22}$$

where

$$f^*(k_n)=\int_0^{h_2} f(r)J_0(k_n r)rdr \tag{3.23}$$

Substituting (3.17) into (3.23), we obtain the transform coefficients as follows

$$f^*(k_n)=J_1(k_n)/k_n \tag{3.24}$$

Substituting (3.18) into (3.23), we obtain the transform coefficients as follows

$$f^*(k_n)=\sum_{l=0}^{\infty}\frac{(-1)^l}{l!}\frac{Q_l}{k_n^{2l+2}} \tag{3.25}$$

where

$$Q_0=h_2k_nJ_1(k_nh_2),\quad Q_l=(h_2k_n)^{2l+1}J_1(k_nh_2)-4l^2Q_{l-1}\qquad(l=1,2,\cdots) \tag{3.26}$$

Accounting for the boundary condition (3.22), let $\Theta^*(k_n, z, t)$ be expressed as follows

$$\Theta^*(k_n,z,t)=\psi g(t)(z-h_1/2)^2+v^*(k_n,z,t) \tag{3.27}$$

where

$$\psi=\frac{f^*(k_n)}{h_1h_2^2J_1^2(k_nh_2)} \tag{3.28}$$

Then we obtain the differential equation on the unknown variable $v^*(k_n, z, t)$ as follows

$$\frac{\partial v^*}{\partial t}=\frac{\partial^2 v^*}{\partial z^2}-k_n^2v^*+2\psi g(t)-\left[\frac{dg(t)}{dt}+k_n^2g(t)\right]\psi(z-h_1/2)^2 \tag{3.29}$$

$$\left.\frac{\partial v^*}{\partial z}\right|_{z=\pm h_1/2}=0 \tag{3.30}$$

$$v^*|_{t=0}=0 \tag{3.31}$$

To solve the Eq. (3.27) together with the boundary condition (3.30) and the initial condition (3.31), we expand $v^*(k_n, z, t)$ in terms of cosine series as follows

$$v^*(k_n,z,t)=\sum_0^{\infty}A_m\cos[h_1\pi m(z+h_1/2)] \tag{3.32}$$

Then we have the differential equation on the unknown variable A_m as follows

$$\frac{dA_m}{dt}+\left[\left(\frac{m\pi}{h_1}\right)^2+k_n^2\right]A_m=\Phi_m^* \tag{3.33}$$

$$A_m|_{t=0}=0 \tag{3.34}$$

where

$$\Phi_0^*=\frac{1}{h_1}\int_{-h_1/2}^{h_1/2}\left\{2g(t)-\left[\frac{dg(t)}{dt}+k_n^2g(t)\right](z-h_1/2)^2\right\}\psi dz \tag{3.35}$$

$$\Phi_m^*=\frac{2}{h_1}\int_{-h_1/2}^{h_1/2}\left\{2g(t)-\left[\frac{dg(t)}{dt}+k_n^2g(t)\right](z-h_1/2)^2\right\}\psi\cos\left[\frac{m\pi}{h_1}(z+h_1/2)\right]dz \tag{3.36}$$

i. e., the equivalent external loading. Because of both free surfaces and the above mentioned temperature difference $\Delta\theta$, the expanding quantity is much more for front surface than for real surface. This makes the irradiated region of the thin plate bulge wholly in the opposite direction of the laser incident direction. Consequently, the equivalent external loading is the key factor to induce the reverse bulge.

Fig. 4 also shows that the maximum value of dimensionless temperature rise on thhe front surface is 9.5×10^{-3}. However, the corresponding factural temperature rise is only $0.78T_m$ in the case of $R_0=0.9$ and $h_4=82.4$, where, we observed that the specimen had completely been perforated. This fact implies that the perforation is caused not by melting but by plugging.

Fig. 5 shows the histories of θ on both surfaces of target at the point $r=0$ for some selected values of h_1, where the shape of pulse laser is of cylindrical type. From the figure, one see that the time t_a increases with the decreasing of h_1^{-1} when $h_1^{-1}<25$, where t_a is the time when the temperature distributions in the axial direction come into agreement. While t_a is almost the same when the $h_1^{-1}>25$. The reason is that t_a is determined by the pulse duration of laser irradiation when the plate is thin. On the other hand, t_a is determined by the heat conduction effects when the plate is thick. Fig. 6 shows the variations of θ with z at selected dimensionless time, where $r=0$ and the spatial shape of laser is of cylindrical type. Again, the characteristics of temperature difference on both surfaces are displayed.

Fig. 7 and Fig. 8 display the dimensionless temperature distributions on the front surface irradiated by spatially cylindrical and Gaussian pulse laser beam respectively. As expected, the temperature response across the irradiated surface generally follows the laser profile. In Fig. 7 the dimensionless temperature is uniform within the laser beam spot and drops sharply near the edge of laser spot even at the later stage of laser irradiation. In Fig. 8 the dimensionless temperature distributions are very similiar to the Gaussian profile with the highest temperature at the centre of the beam, i.e. $r=0$, and the lowest temperatures near the edge of the profile. Unlike in Fig. 7, the temperatures drops smoothly in the radial direction and there is not the region of a severe temperature change in Fig. 8.

Fig. 9 and Fig. 10 show the temperature gradient distributions on the front surface irradiated by spatially cylindrial and Gaussian shape pulse laser beam respectively. A comparison of Fig. 9 with Fig. 10 reveals that the distributions of temperature gradient are extremely different, although the net energy content in the material at each time is the same for both cases. Fig. 9 predicts that the radial temperature gradients vary severely in a ring whose dimensionless radius is 1, i.e., the radius of laser spot. While Fig. 10 predicts that the radial temperature gradients vary smoothly and their maximum values are in a ring whose dimensionless radius is $\sqrt{2}/2$, i.e., $r_{max}=\sqrt{2}/2$. The maximum temperature gradients in Fig. 9 are 40 times larger than that in Fig. 10. From the temperature and its gradient distributions, one sees readily that the temperature discontinuity makes the irradiated region of the foil bulge wholly in the opposite direction of laser incident direction when the spatial shape of laser is of cylindrical type, while the non-irradiated region of the foil is almost static. Consequently the reverse bulge motion or the deformation of thin plate is discontinuous on the rim of laser spot. Because of this discontinuity, the laser beam with spatially cylindrical distribution offers a formidable potential for the RPE in the metallic foils. Howerver, the temperature, temperature gradient and reverse-bulge motion of thin plate are continuous in the radial direction when the spatial shape of laser is of Gaussian type.

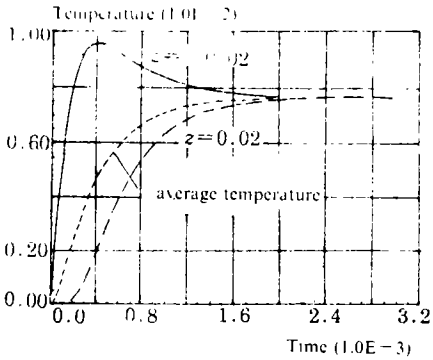

Fig. 4 The histories of θ on both surfaces of thin plate at the point $r=0$

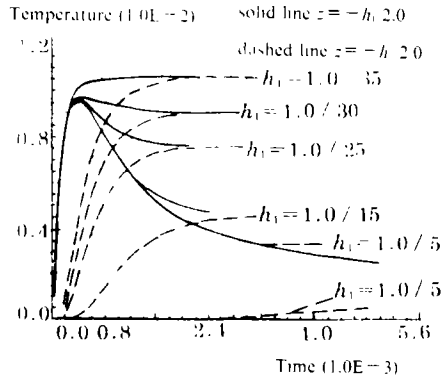

Fig. 5 The histories of θ on both surfaces of target at the point $r=0$ for some selected values of h_1

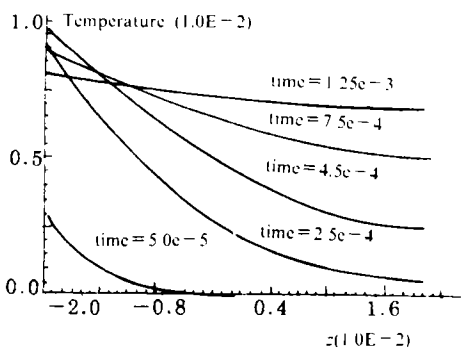

Fig. 6 The variations of θ with z at selected dimensionless time, where $r=0$ and the spatial shape of laser is of cylindrical type ($r=0$, $h_1=1.0/25$)

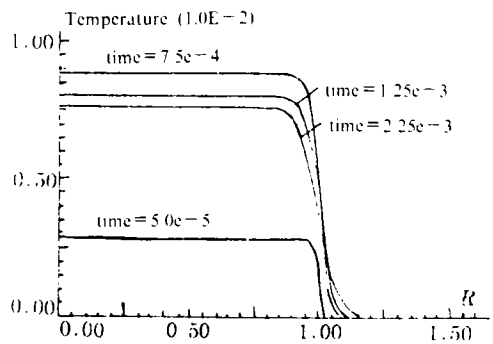

Fig. 7 The dimensionless temperature distributions on the front surface irradiated by spatially cylindrical pulse laser beam

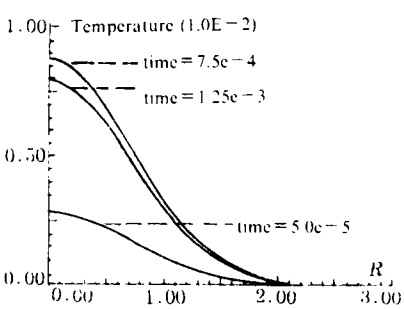

Fig. 8 The dimensionless temperature distributions on the front surface irradiated by Gaussian pulse laser beam

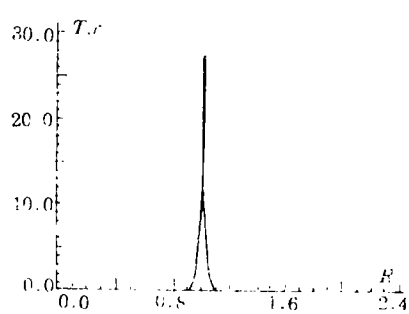

Fig. 9 The temperature gradient distributions on the front surface irradiated by spatially cylindrial shape pulse laser beam

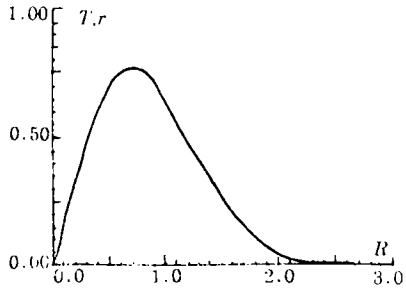

Fig. 10 The temperature gradient distributions on the front surface irradiated by Gaussian shape pulse laser beam

V. Concluding Remarks

In this paper the temperature distributions in the metallic foils induced by spatially cylindrical shape long-pulse laser beam are examined in order to analyse the RPE. Under some reasonable assumptions, the exact solution of temperture fields is derived by using the Hankel transform. Numerical results are presented for a given temporal and spatial distribution of laser beam. We can draw the following conclusion from the analysis of the temperature fields: (1) The temperature gradients in the axial direction are the key factor to induce the reverse bulge motion of the thin plate. (2) The temperature discontinuity in the radial direction on the rim of laser spot is the key factor to cause shear deformation localization. Comparing the temperature distribution in metallic foils induced by spatially cylindrical with that induced by Gaussian type laser beam, the former offers a formidable potential for the RPE, however, the latter has little potential for the RPE.

In the present analysis, the thermophysical properties are assumed to be constant so that analytical solutions to the problem may be obtained. In reality, the material properties, especially the reflective, vary with temperature. But for these cases the problem should be solved by purely numerical approaches. Besides this, the assumption, which the present problems are studied in a static coordinate system and the temperature deformation of thin plate is uncoupled, may be a certain effect on temperature distributions.

References

[1] S. Eliezer, I. Gilath and T. Bar-Noy, Laser-induced spall in metals: experiment and simulation, *J. Appl. Phys.*, **67**, 2 (1990), 715－724.

[2] M. Boustie and F. Cottet, Experimental and numerical study of laser induced spallation into aluminum and copper targets, *J. Appl. Phys.*, **69**, 11 (1991), 7533－7538.

[3] A. D. Zweig, A thermo-mechanical model for laser ablation, *J. Appl. Phys.* **70**, 3 (1991), 1684－1691.

[4] S. S. Cohen, J. B. Bernstein and P. W. Wyatt, The effect of multiple laser pulses on damage to thin metallic films, *J. Appl. Phys.*, **71**, 2 (1992), 630－637.

[5] A. Kar and J. Mazumder, Two-dimensional model for materials damage due to melting and vaporization during laser irradiation, *J. Appl. Phys.*, **68**, 8 (1990), 3884－3891.

[6] C. W. Sun, Analysis of damage mechanisms for materials and structures irradiated by power laser beam, *Proceedings of the Symposium on Laser Thermal and Mechanical Effects*, Shanghai (1991).

[7] Z. P. Duan, Y. C. Zhou and C. Q. Wang, Reverse-plugging effect in metallic foils induced by non Gaussian pulse laser beam, *Proceedings of the Symposium on Laser Thermal and Mechanical Effects*, Chengdu (1992), 434—453. (in Chinese)

[8] Z. P. Duan and Y. C. Zhou, Reverse-plugging effect in metallic foils induced by long pulse laser beam, *Advances in Mechanics*, **23**, 1 (1993), 11, (in Chinese)

[9] Z. P. Duan, C. Q. Wang and Y. C. Zhou, Manufacture and its application of multi-function Nd: Glass pulse laser equipment, *Proceedings of the Symposium on Laser Thermal and Mechanical Effects*, Chengdu (1992), 579—587. (in Chinese)